Particle-hole induced electric and magnetic rotation in ^{111}In

P. Vaska,* D. B. Fossan, D. R. LaFosse, H. Schnare,† and M. P. Waring
Department of Physics, State University of New York at Stony Brook, Stony Brook, New York 11794

S. M. Mullins,‡ G. Hackman,§ D. Prévost, and J. C. Waddington
Department of Physics and Astronomy, McMaster University, Hamilton, Ontario, Canada L8S 4M1

V. P. Janzen and D. Ward**
AECL Research, Chalk River Laboratories, Chalk River, Ontario, Canada K0J 1J0

R. Wadsworth
Department of Physics, University of York, Heslington, York YO1 5DD, United Kingdom

E. S. Paul
Oliver Lodge Laboratory, University of Liverpool, P.O. Box 147, Liverpool L69 7ZE, United Kingdom
(Received 3 November 1997)

The high-spin structure of ^{111}In has been investigated with γ-ray spectroscopic methods using the ^{96}Zr(^{19}F,4n) reaction with thin and backed targets. A comprehensive level scheme has been constructed which exhibits interesting collective as well as novel single-particle excitations. Unambiguous evidence of proton particle-hole excitations is found for the first time in a $Z<50$ nucleus in the form of decoupled bands involving proton $g_{7/2}(d_{5/2})$ and $h_{11/2}$ orbitals above the $Z=50$ spherical shell gap. The high-spin structure of ^{111}In also involves the recently discovered magnetic rotation mechanism which is manifest as high-spin $\Delta I=1$ bands with no signature splitting and large $B(M1)$ strengths, but only a small associated deformation. [S0556-2813(98)03604-8]

PACS number(s): 21.10.Re, 23.20.Lv, 25.70.Gh, 27.60.+j

I. INTRODUCTION

In recent years, considerable progress has been made in the identification and theoretical interpretation of rotational bands in nuclei just above the $Z=50$ proton shell gap. The study of rotational structures in nuclei usually considered to be spherical is critical to an understanding of the coexistence of, and transition between, deformed and spherical nuclear shapes. Prolate deformations in $Z=50$ Sn, $Z=51$ Sb, and $Z=52$ Te nuclei appear to be stabilized by proton particle-hole (p-h) excitations across the $Z=50$ shell gap, with the holes invariably in the high-Ω orbitals of the $g_{9/2}$ subshell, and the particles in one or more of the low-Ω orbitals of the next major shell, i.e., in the $g_{7/2}$, $d_{5/2}$, or $h_{11/2}$ orbitals. The neutron Fermi level is also in this major shell, albeit at a higher energy. These excitations are believed to be responsible for intruder-type rotational bands extending to some of the highest spins and excitation energies ever observed in nuclei.

Bands in these various nuclei near the $Z=50$ proton shell closure can be classified according to the number of proton p-h excitations involved in their configurations. For example, $1p$-$1h$ excitations in $Z=51$ Sb nuclei give rise to high-K strongly coupled bands of modest deformation based on the $\pi g_{9/2}$ hole orbital [1,2]. This is referred to as a $2p1h$ configuration, where it is implied that the configuration is relative to the Sn core. Bands based on $2p$-$2h$ excitations have larger deformations and are found in several of the Sn, Sb, and Te isotopes [3–8]. The deformations associated with these configurations are strongly affected by the well-known level crossing between the downsloping $\pi g_{7/2}$ and upsloping $\pi g_{9/2}$ orbitals at a quadrupole deformation of $\beta_2 \sim 0.20$.

In addition, a unique phenomenon called smooth band termination [9,10] has been discovered in some of the intruder bands resulting from these deformations. The process involves a gradual change in the shape of the nucleus with increasing spin from collective prolate ($\gamma=0°$) to noncollective oblate ($\gamma=+60°$) as the spins of all valence particles outside of the doubly magic ^{100}Sn core (plus proton holes) become aligned. Since, at the noncollective oblate shape, the total spin of the nucleus is composed only of contributions from occupied single-particle orbits, the spin associated with a particular configuration cannot exceed a certain maximum value. This can be observed as a termination of the band sequence at that spin as long as the sequence of states corresponding to that particular configuration lies sufficiently close to the yrast line that it is populated in the formation and

*Current address: UGM Laboratory, Inc., 3611 Market St., Philadelphia, PA 19104.

†Current address: Institut für Kern- und Teilchenphysik, TU Dresden, Mommsenstr. 13, D-01062 Dresden, Germany.

‡Current address: Department of Nuclear Physics, Australian National University, GPO Box 4, Canberra ACT 2601, Australia.

§Current address: Argonne National Laboratory, Argonne, IL 60439.

**Current address: Nuclear Science Division, Lawrence Berkeley National Laboratory, Berkeley, CA 94720.

decay of the nucleus. Above the $Z=50$ gap, a number of cases have been identified in which one or more configurations meet these criteria and the entire sequence up to the terminating state has been observed. This feature has been addressed theoretically with considerable success [10], and the decrease in collectivity with increasing spin has recently been verified by experiment [11].

Given the richness of collective and noncollective behavior in nuclei at and above the $Z=50$ gap, it is of special interest to determine whether analogous structures exist below the gap. To pursue this investigation, the $Z=49$ In nuclei are particularly suitable largely because certain proton $1p$-$1h$ excitations across the gap can be easily identified without reliance on comparisons with complex theoretical models, as is often the case with even-Z nuclei in this region. All configurations in indium nuclei involving an odd number of $g_{9/2}$ proton holes will have a large K value, and are expected to be nearly signature degenerate. Only the promotion of a $g_{9/2}$ proton to a low-Ω intruder orbital, namely, the proton $1p$-$1h$ excitation leaving a $g_{9/2}$ proton hole pair, provides the conditions necessary for the occurrence of decoupled rotational bands: upsloping proton-hole orbitals and a downsloping proton orbital to drive the core to a deformed prolate shape, and a low K value for the configuration to achieve a large signature splitting. This situation is complementary to the odd-mass $Z=51$ Sb nuclei, in which the existence of high-K strongly coupled bands can be unambiguously associated with a $1p$-$1h$ excitation from the $g_{9/2}$ orbital below the shell gap.

In contrast, the interpretation of rotational bands in even-Z Cd ($Z=48$), Sn, and Te nuclei is more subtle, since p-h excitations do not have such a clear signature. Much of the support for the p-h interpretations of bands in the Sn and Te nuclei relies on comparisons with, for example, the smooth band termination calculations mentioned earlier. Recent experimental investigations of the even-mass $Z=48$ Cd nuclei [12–15] have uncovered various rotational structures, but it has been difficult to demonstrate the involvement of p-h excitations and this interpretation continues to be questioned [13,16].

Before this work, no convincing evidence of any rotational behavior had been found in indium nuclei. The ^{111}In nucleus in particular is expected to be a good candidate for the observation of these phenomena since its neutron Fermi surface (at $N=62$) is near midshell where deformed shapes are most favored, but low enough that the number of valence neutrons does not preclude the observation of smooth band termination. The initial publication from this work [17] presented the discovery of the first proton intruder band in a nucleus below the $Z=50$ gap, which is based on the $\pi h_{11/2}$ orbital via a $1p$-$1h$ proton excitation of the core. The present paper reports a complete analysis of the data and the discovery of additional intruder bands.

II. EXPERIMENTAL DETAILS

Three separate experiments were performed, all using the ^{96}Zr(^{19}F,$4n$) reaction to populate high-spin states in ^{111}In. A backed-target experiment provided maximum energy resolution for most γ-ray transitions and the highest statistics. The target consisted of 2 mg/cm^2 of ^{96}Zr backed by 15 mg/cm^2 of ^{208}Pb. The beam was provided by the Stony Brook FN Tandem/Superconducting LINAC facility, and its energy was chosen to be 72 MeV, determined by an excitation function to maximize the yield of ^{111}In. Coincident γ rays were detected by the Stony Brook array of six Compton-suppressed high-purity Ge detectors (of $\sim$ 25% efficiency) and a 14-element bismuth germanate (BGO) multiplicity (K)/ sum-energy (H) filter with a hardware requirement of $K\geqslant 2$. A total of 157×10^6 $\gamma-\gamma$ events were recorded using a coincidence resolving time of $2\tau=100$ ns. The data were sorted into symmetrized and angular correlation $\gamma-\gamma$ matrices for offline analysis.

A more sensitive investigation of the structure at the highest spins was made possible by a second, thin-target experiment. The target was self-supporting with a thickness of 500 μg/cm^2, giving good energy resolution for γ-ray decays of short-lived high-spin states. The population and detection of high-spin states were enhanced by employing a higher beam energy of 85 MeV and the improved resolving power of the 8π γ-ray spectrometer at the TASCC facility in Chalk River, which consisted of 20 Compton-suppressed high purity Ge detectors and a 71-element BGO K/H filter set at $K\geqslant 5$. A total of 50×10^6 $\gamma-\gamma$ events were recorded, from which a symmetrized $\gamma-\gamma$ matrix was sorted using a minimum H cut of 13.4 MeV to enhance ^{111}In ($4n$) over ^{110}In ($5n$).

A third experiment was performed, again using the 8π spectrometer, to measure mean lifetimes of band members of the strongest intruder band using the Doppler-shift attenuation method (DSAM) [18]. In this case, the target was 600 μg/cm^2 thick with a 15 mg/cm^2 ^{197}Au backing, the beam energy was again 85 MeV, and 296×10^6 $\gamma-\gamma$ events were collected.

III. DATA ANALYSIS AND RESULTS

The level scheme of ^{111}In was constructed on the basis of observed coincidence and intensity relationships using both

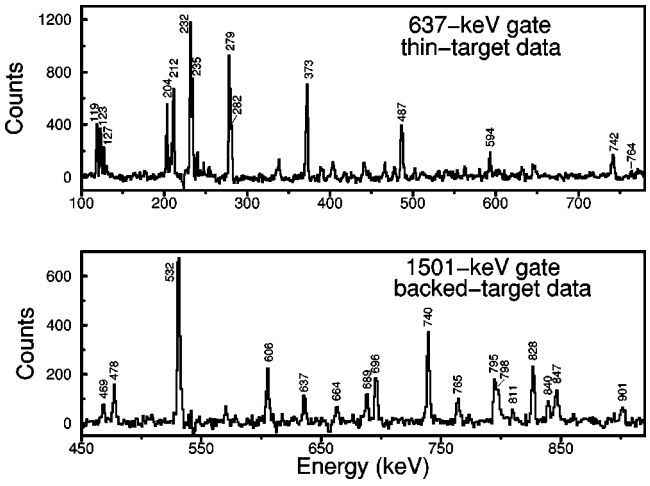

FIG. 1. Background-subtracted γ-ray spectra gated on the 637-keV transition from the thin-target data (top), and the 1501-keV transition from the Stony Brook backed-target data (bottom). Peaks identified with band 6 and its decay (top) and with bands 2 and 3 (bottom) are labeled with their transition energies in keV. Unlabeled peaks belong to weaker, less significant decay paths or are contaminants from nuclei populated in other reaction channels.

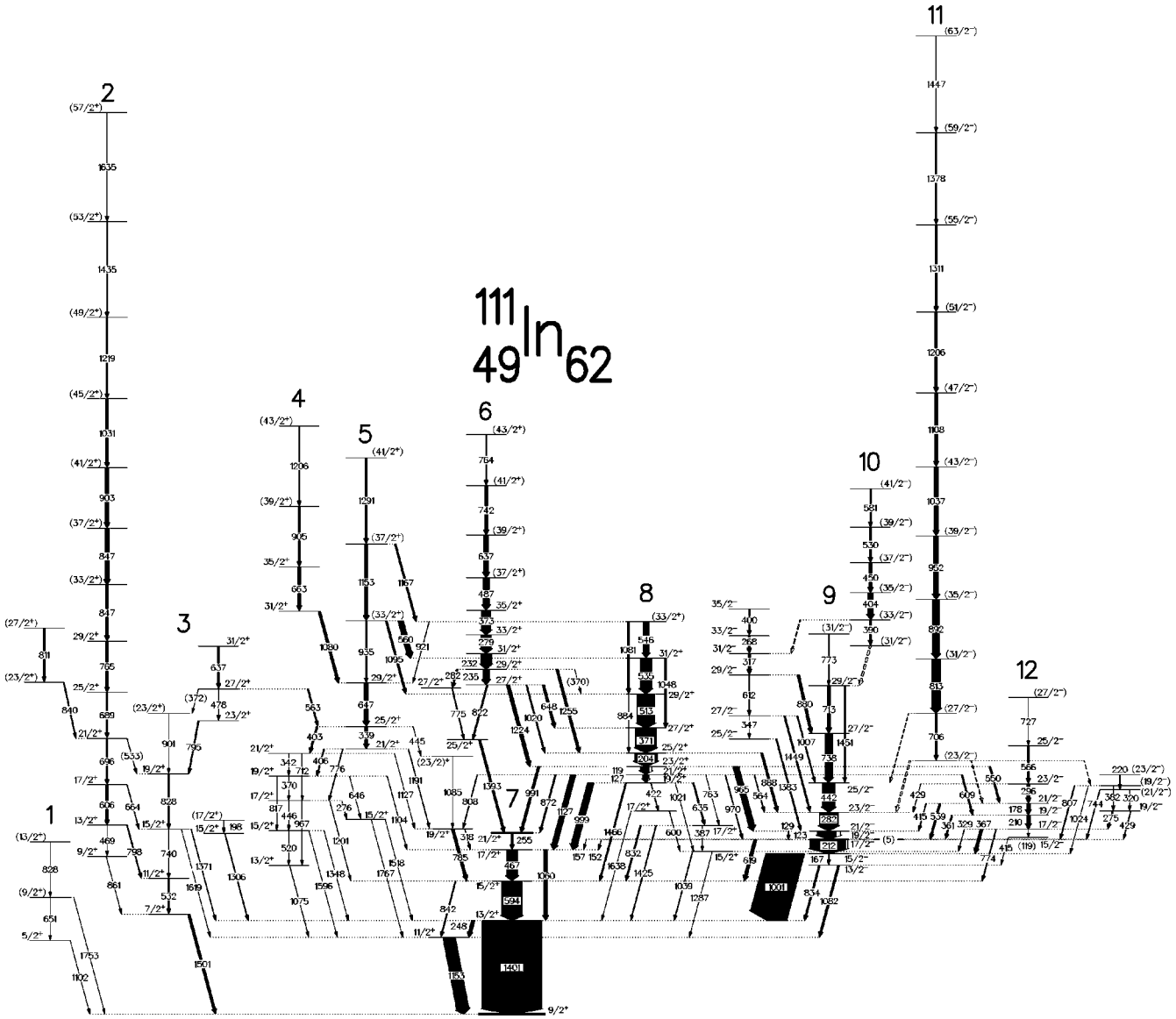

FIG. 2. Level scheme of ^{111}In as determined from the present series of experiments. The filled portion of the transition arrow width is proportional to the coincidence γ-ray intensity observed in the thin-target data corrected for detector efficiency, while the open portion indicates the expected additional (unobserved) transition intensity from internal electron conversion. Parentheses indicate tentative assignment for spins and parities, and tentative observation for γ rays.

the backed- and thin-target matrices. A relevant spectrum from each matrix is shown in Fig. 1. The DSAM data were not optimized for this purpose, but their consistency with the proposed level scheme was confirmed. The RADWARE software package [19] was particularly helpful in fitting the transition energies and relative coincidence intensities, which are given in Table I, as well as for keeping account of the contaminating γ rays from competing reaction channels which were mainly those to ^{110}In and ^{110}Cd. Previously, experiments using lighter ions [20–25] established many of the observed levels up to about 3 MeV in excitation energy. The present data confirm many of these proposed levels and considerably extend the known level scheme.

It was assumed that, in general, levels decay to those with lower spin, and that prompt γ-ray decays between states of the same parity are constrained to $\Delta I \leqslant 2$, and those between states of opposite parity to $\Delta I \leqslant 1$. In addition to these standard assumptions, the method of directional correlation from oriented states (DCO) [26] was employed to assign spin and parity values to new levels, using the firm assignments of previously established levels as a starting point. From the Stony Brook backed-target data, γ-ray pairs consisting of one from a detector at 90° relative to the beam direction and another from a 35° detector, were sorted into an $E_{\gamma,35°}$ vs $E_{\gamma,90°}$ DCO matrix. Gates were set at energies of known pure dipole or quadrupole transitions, and projected onto both axes. For γ rays coincident with the gating transitions, DCO ratios $I_{\gamma,35°}/I_{\gamma,90°}$ were determined, where $I_{\gamma,35°}$ is the γ intensity measured from the gate projected onto the 35° axis, and $I_{\gamma,90°}$ the intensity from the 90° projection. Assigned transition multipolarities were required to be consistent with measured DCO ratios, which are listed in Table I for all γ rays for which a value could be determined. When gating on a known stretched $E2$ transition, a ratio of 1.0 is typical for

TABLE I. Energies, relative coincidence intensities, DCO ratios, initial and final state spins, and multipolarities of transitions assigned to ^{111}In in the present series of experiments.

E_γ (keV)	$I_{\gamma,\mathrm{thin}}$[a] (%)	$I_{\gamma,\mathrm{backed}}$[b] (%)	DCO Ratio[c]	$I_i^\pi \rightarrow I_f^\pi$	Multipolarity
(5.0)				$19/2^- \rightarrow 17/2^-$	$M1/E2$
(118.8)				$17/2^- \rightarrow 15/2^-$	$M1/E2$
118.8(1)	14.9(8)	6.6(3)	0.50(2)	$23/2^+ \rightarrow 21/2^+$	$M1/E2$
123.5(1)	31.7(1.6)	18.4(9)	0.48(1)	$21/2^- \rightarrow 19/2^-$	$M1/E2$
127.4(1)	8.1(4)	3.5(2)	0.47(2)	$21/2^+ \rightarrow 19/2^+$	$M1/E2$
128.8(1)	0.9(1)	0.9(1)		$21/2^- \rightarrow 17/2^-$	$E2$
152.2(2)	0.3(1)	0.2(1)	1.04(52)	$17/2^- \rightarrow 17/2^+$	$E1$
157.1(2)	0.2(1)	0.2(1)	0.63(26)	$19/2^- \rightarrow 17/2^+$	$E1$
166.9(1)	1.2(1)	1.1(1)	1.14(8)[d]	$15/2^- \rightarrow 13/2^-$	$M1/E2$
177.8(1)	5.1(3)	3.3(2)	0.48(2)	$21/2^- \rightarrow 19/2^-$	$M1/E2$
197.7(1)	0.6(1)	0.5(1)		$(17/2^+) \rightarrow 15/2^+$	$(M1/E2)$
204.1(1)	36.0(1.8)	17.4(9)	0.43(1)	$25/2^+ \rightarrow 23/2^+$	$M1/E2$
210.4(1)	5.2(4)	3.2(2)		$19/2^- \rightarrow 17/2^-$	$M1/E2$
211.7(1)	60.2(3.1)	43.3(2.2)	0.49(1)	$17/2^- \rightarrow 15/2^-$	$M1/E2$
219.6(1)	1.2(1)	0.5(1)		$(23/2^-) \rightarrow (21/2^-)$	$(M1/E2)$
232.0(1)	17.4(9)	6.5(3)	0.45(2)	$31/2^+ \rightarrow 29/2^+$	$M1/E2$
234.8(1)	10.3(5)	4.1(2)	0.45(2)	$29/2^+ \rightarrow 27/2^+$	$M1/E2$
248.1(1)	5.4(4)	4.6(2)	0.49(8)	$13/2^+ \rightarrow 11/2^+$	$M1/E2$
255.3(1)	3.0(1)	10.4(5)	0.90(3)	$21/2^+ \rightarrow 17/2^+$	$E2$
268.2(1)	3.4(2)	1.9(1)	0.45(4)	$33/2^- \rightarrow 31/2^-$	$M1/E2$
274.9(1)	1.7(1)	1.1(1)	0.48(6)[e]	$19/2^- \rightarrow 17/2^-$	$M1/E2$
276.1(1)	0.2(1)	0.4(1)	0.59(11)	$17/2^+ \rightarrow 15/2^+$	$M1/E2$
279.3(1)	17.1(9)	5.9(3)	0.39(2)	$33/2^+ \rightarrow 31/2^+$	$M1/E2$
281.7(1)	30.6(1.5)	19.1(1.0)	0.44(1)	$23/2^- \rightarrow 21/2^-$	$M1/E2$
282.1(1)	2.7(2)	1.2(1)	0.48(6)	$29/2^+ \rightarrow 27/2^+$	$M1/E2$
295.7(1)	4.3(2)	3.2(2)	0.41(3)	$23/2^- \rightarrow 21/2^-$	$M1/E2$
317.3(1)	3.9(2)	2.1(1)	0.50(4)	$31/2^- \rightarrow 29/2^-$	$M1/E2$
318.3(1)	0.7(1)	0.8(1)	0.57(10)	$19/2^+ \rightarrow 17/2^+$	$M1/E2$
319.6(1)	0.7(1)	0.6(1)		$(21/2^-) \rightarrow 19/2^-$	$(M1/E2)$
328.8(2)	0.3(1)	0.4(1)		$17/2^- \rightarrow 15/2^+$	$E1$
339.1(1)	5.3(3)	2.5(1)	0.92(8)	$25/2^+ \rightarrow 21/2^+$	$E2$
341.8(1)	0.1(1)	0.7(1)	0.79(11)	$21/2^+ \rightarrow 19/2^+$	$M1/E2$
347.4(1)	0.4(1)	0.3(1)	0.66(7)[d]	$27/2^- \rightarrow 25/2^-$	$M1/E2$
360.7(1)	2.2(2)	1.7(1)	0.82(9)	$19/2^- \rightarrow 19/2^-$	$M1/E2$
366.8(1)	4.6(4)	5.3(3)	0.63(3)	$17/2^- \rightarrow 15/2^-$	$M1/E2$
(369.6)				$29/2^+ \rightarrow 29/2^+$	$M1/E2$
370.4(1)	0.1(1)	1.2(1)	0.75(13)	$19/2^+ \rightarrow 17/2^+$	$M1/E2$
371.3(1)	34.9(1.8)	14.2(7)	0.42(3)	$27/2^+ \rightarrow 25/2^+$	$M1/E2$
(371.6)				$27/2^+ \rightarrow (23/2^+)$	$(E2)$
372.9(1)	15.7(8)	4.2(2)	0.48(2)	$35/2^+ \rightarrow 33/2^+$	$M1/E2$
381.8(1)	0.7(1)	0.4(1)		$(19/2^-) \rightarrow 19/2^-$	$(M1/E2)$
386.7(9)		0.1(1)		$17/2^+ \rightarrow 15/2^+$	$M1/E2$
390.5(1)	2.7(2)	0.4(1)	0.24(8)[d]	$(33/2^-) \rightarrow (31/2^-)$	$(M1/E2)$
399.9(1)	2.5(1)	0.9(1)	0.62(5)[d]	$35/2^- \rightarrow 33/2^-$	$M1/E2$
402.7(1)	2.7(2)	1.3(1)	0.98(10)	$25/2^+ \rightarrow 21/2^+$	$E2$
404.2(1)	9.2(5)	1.2(1)	0.44(4)[d]	$(35/2^-) \rightarrow (33/2^-)$	$(M1/E2)$
405.6(1)	1.5(2)	1.2(1)	0.58(4)	$21/2^+ \rightarrow 19/2^+$	$M1/E2$
415.0(1)	0.9(1)	0.7(1)	1.62(21)[d]	$21/2^- \rightarrow 21/2^-$	$M1/E2$
415.1(2)		0.4(1)	1.18(28)[d]	$15/2^- \rightarrow 13/2^-$	$M1/E2$
421.7(3)	0.8(1)	0.2(1)	0.21(13)[d]	$19/2^+ \rightarrow 17/2^+$	$M1/E2$
428.5(2)	0.3(1)	0.2(1)	1.41(40)[d]	$23/2^- \rightarrow 23/2^-$	$M1/E2$
429.5(1)	0.9(1)	0.6(1)	0.75(11)[d]	$19/2^- \rightarrow 17/2^-$	$M1/E2$
442.0(1)	21.2(1.1)	10.7(5)	0.37(1)	$25/2^- \rightarrow 23/2^-$	$M1/E2$
445.2(2)		0.3(1)		$25/2^+ \rightarrow (23/2^+)$	$(M1/E2)$

TABLE I. (*Continued*).

E_γ (keV)	$I_{\gamma,\text{thin}}$[a] (%)	$I_{\gamma,\text{backed}}$[b] (%)	DCO Ratio[c]	$I_i^\pi \rightarrow I_f^\pi$	Multipolarity
446.5(1)	0.5(2)	1.2(1)	0.64(9)	$17/2^+ \rightarrow 15/2^+$	$M1/E2$
449.6(1)	4.9(3)	0.5(1)		$(37/2^-) \rightarrow (35/2^-)$	$(M1/E2)$
466.9(1)	18.1(1.0)	16.6(8)	0.55(1)	$17/2^+ \rightarrow 15/2^+$	$M1/E2$
468.9(2)		0.2(1)	1.09(21)	$13/2^+ \rightarrow 9/2^+$	$E2$
478.0(1)	0.9(1)	0.7(1)		$27/2^+ \rightarrow 23/2^+$	$E2$
487.1(1)	10.7(6)	1.7(1)		$(37/2^+) \rightarrow 35/2^+$	$(M1/E2)$
513.2(1)	29.7(1.5)	9.0(5)	0.40(2)	$29/2^+ \rightarrow 27/2^+$	$M1/E2$
520.2(2)		0.2(1)		$15/2^+ \rightarrow 13/2^+$	$M1/E2$
529.8(1)	3.0(2)	0.1(1)		$(39/2^-) \rightarrow (37/2^-)$	$(M1/E2)$
531.7(1)	2.4(4)	1.9(1)	0.87(10)	$11/2^+ \rightarrow 7/2^+$	$E2$
(533.2)				$21/2^+ \rightarrow 19/2^+$	$M1/E2$
534.9(1)	19.4(1.0)	4.4(2)		$31/2^+ \rightarrow 29/2^+$	$M1/E2$
538.6(1)	3.0(2)	2.4(1)	1.04(14)[d]	$21/2^- \rightarrow 19/2^-$	$M1/E2$
546.4(1)	9.0(5)	1.5(1)		$(33/2^+) \rightarrow 31/2^+$	$(M1/E2)$
549.8(1)	2.6(1)	1.4(1)	0.82(19)[d]	$23/2^+ \rightarrow 21/2^-$	$E1$
559.9(1)	8.9(5)	1.1(1)		$(33/2^+) \rightarrow 31/2^+$	$(M1/E2)$
562.9(1)	2.0(2)	1.0(1)	0.34(5)	$27/2^+ \rightarrow 25/2^+$	$M1/E2$
563.9(1)	0.8(1)	0.6(1)	0.97(9)[d]	$21/2^+ \rightarrow 23/2^-$	$E1$
565.7(1)	2.9(2)	1.7(1)	0.56(7)	$25/2^- \rightarrow 23/2^-$	$M1/E2$
580.5(1)	2.3(2)			$(41/2^-) \rightarrow (39/2^-)$	$(M1/E2)$
593.6(1)	34.2(2.0)	25.4(1.3)	0.58(1)	$15/2^+ \rightarrow 13/2^+$	$M1/E2$
599.6(2)	0.4(3)	0.5(1)		$17/2^+ \rightarrow 15/2^+$	$M1/E2$
605.9(1)	3.3(4)	1.4(1)	0.95(14)	$17/2^+ \rightarrow 13/2^+$	$E2$
609.1(2)	2.3(1)	0.4(1)	0.72(16)[d]	$21/2^+ \rightarrow 19/2^-$	$E1$
611.5(1)	1.9(1)	0.7(1)	0.59(19)[d]	$29/2^- \rightarrow 27/2^-$	$M1/E2$
619.4(1)	5.0(1.0)	2.1(1)	0.51(5)	$17/2^- \rightarrow 15/2^+$	$E1$
634.8(1)	2.0(2)	0.8(1)	0.78(11)[d]	$19/2^+ \rightarrow 17/2^+$	$M1/E2$
636.5(1)	2.7(3)	1.7(1)	0.98(18)	$31/2^+ \rightarrow 27/2^+$	$E2$
637.1(1)	8.2(4)	0.7(1)		$(39/2^+) \rightarrow (37/2^+)$	$(M1/E2)$
646.3(2)		0.7(1)	0.94(7)[e]	$19/2^+ \rightarrow 15/2^+$	$E2$
646.8(1)	7.0(4)	3.2(2)	0.94(7)[e]	$29/2^+ \rightarrow 25/2^+$	$E2$
648.4(1)	3.9(2)	1.0(1)	1.38(23)[d]	$27/2^+ \rightarrow 27/2^+$	$M1/E2$
651.1(2)		0.3(1)		$(9/2^+) \rightarrow 5/2^+$	$(E2)$
663.3(1)	4.0(7)	0.7(1)	1.05(21)	$35/2^+ \rightarrow 31/2^+$	$E2$
663.9(1)	0.7(2)	0.5(1)	0.14(11)	$17/2^+ \rightarrow 15/2^+$	$M1/E2$
688.7(1)	2.2(2)	1.1(1)	0.97(11)	$25/2^+ \rightarrow 21/2^+$	$E2$
696.4(1)	2.3(3)	1.5(1)	0.94(8)	$21/2^+ \rightarrow 17/2^+$	$E2$
705.7(2)	3.0(2)	0.4(1)	1.93(32)[d]	$(27/2^-) \rightarrow (23/2^-)$	$(E2)$
712.4(1)	0.1(1)	0.9(1)	0.98(18)	$21/2^+ \rightarrow 17/2^+$	$E2$
713.1(1)	4.9(3)	1.5(1)		$29/2^- \rightarrow 27/2^-$	$M1/E2$
726.5(2)	0.4(1)	0.3(1)		$(27/2^-) \rightarrow 25/2^-$	$(M1/E2)$
738.0(1)	13.2(7)	5.9(3)	0.42(2)	$27/2^- \rightarrow 25/2^-$	$M1/E2$
740.1(1)	1.2(3)	1.4(1)	1.08(11)	$15/2^+ \rightarrow 11/2^+$	$E2$
741.9(1)	4.7(3)			$(41/2^+) \rightarrow (39/2^+)$	$(M1/E2)$
744.4(1)	0.7(1)	1.1(1)		$(21/2^-) \rightarrow 19/2^-$	$(M1/E2)$
762.6(4)		0.1(1)		$21/2^+ \rightarrow 17/2^+$	$E2$
764.0(2)	1.6(1)			$(43/2^+) \rightarrow (41/2^+)$	$(M1/E2)$
764.7(1)	3.8(4)	1.5(1)	0.84(12)	$29/2^+ \rightarrow 25/2^+$	$E2$
773.2(3)	1.0(1)	0.4(1)		$(31/2^-) \rightarrow 29/2^-$	$(M1/E2)$
774.1(3)	1.2(1)	0.4(1)		$17/2^- \rightarrow 15/2^+$	$E1$
774.7(1)	1.3(3)	1.5(1)	0.52(6)	$27/2^+ \rightarrow 25/2^+$	$M1/E2$
775.9(1)	0.9(2)	0.7(1)	0.97(13)	$21/2^+ \rightarrow 17/2^+$	$E2$
785.4(1)	4.4(4)	3.3(2)	1.04(11)	$19/2^+ \rightarrow 15/2^+$	$E2$
795.5(1)	1.7(3)	1.2(1)	1.00(13)	$23/2^+ \rightarrow 19/2^+$	$E2$

TABLE I. (*Continued*).

E_γ (keV)	$I_{\gamma,\text{thin}}$[a] (%)	$I_{\gamma,\text{backed}}$[b] (%)	DCO Ratio[c]	$I_i^\pi \rightarrow I_f^\pi$	Multipolarity
798.2(1)	1.3(3)	0.5(1)	0.51(7)	$13/2^+ \rightarrow 11/2^+$	$M1/E2$
806.7(2)	1.3(3)	1.2(1)	0.80(12)[e]	$(19/2^-) \rightarrow 19/2^-$	$(M1/E2)$
808.4(2)	0.9(1)	0.5(1)	0.80(12)[e]	$21/2^+ \rightarrow 19/2^+$	$M1/E2$
811.0(1)	2.2(3)	0.5(1)		$(27/2^+) \rightarrow (23/2^+)$	$(E2)$
813.2(1)	14.3(9)	0.6(1)		$(31/2^-) \rightarrow (27/2^-)$	$(E2)$
816.5(2)	0.1(1)	0.3(1)		$19/2^+ \rightarrow 15/2^+$	$E2$
822.3(1)	2.3(2)	0.5(1)	0.50(11)	$27/2^+ \rightarrow 25/2^+$	$M1/E2$
827.7(1)	2.2(4)	1.6(1)	0.98(13)	$19/2^+ \rightarrow 15/2^+$	$E2$
828.0(2)		0.4(1)		$(13/2^+) \rightarrow (9/2^+)$	$(E2)$
832.3(3)	2.2(4)	0.4(1)		$17/2^+ \rightarrow 15/2^+$	$M1/E2$
834.2(2)	2.5(6)	0.9(1)	1.34(14)[d]	$13/2^- \rightarrow 13/2^+$	$E1$
840.2(1)	1.5(2)	0.8(1)	0.80(18)	$(23/2^+) \rightarrow 21/2^+$	$(M1/E2)$
842.0(1)	1.6(2)	1.7(1)	1.32(24)	$15/2^+ \rightarrow 11/2^+$	$E2$
846.8(2)	4.0(3)	1.2(1)		$(33/2^+) \rightarrow 29/2^+$	$(E2)$
847.5(3)	7.5(5)	1.1(1)		$(37/2^+) \rightarrow (33/2^+)$	$(E2)$
861.4(3)		0.1(1)	0.66(17)	$9/2^+ \rightarrow 7/2^+$	$M1/E2$
871.7(2)	2.0(3)	0.7(1)	1.11(11)	$21/2^+ \rightarrow 21/2^+$	$M1/E2$
880.3(1)	4.1(3)	1.7(1)	0.62(10)	$29/2^- \rightarrow 27/2^-$	$M1/E2$
884.3(2)	1.2(2)	0.3(1)	1.05(23)[d]	$29/2^+ \rightarrow 25/2^+$	$E2$
887.6(1)	3.4(2)	1.0(1)	0.93(19)[d]	$25/2^+ \rightarrow 23/2^-$	$E1$
891.7(1)	11.6(7)	0.3(1)		$(35/2^-) \rightarrow (31/2^-)$	$(E2)$
901.1(2)		0.3(1)		$(23/2^+) \rightarrow 19/2^+$	$(E2)$
902.8(1)	5.1(4)	0.5(1)		$(41/2^+) \rightarrow (37/2^+)$	$(E2)$
905.0(1)	3.6(2)	0.6(1)		$(39/2^+) \rightarrow 35/2^+$	$(E2)$
921.3(2)	0.3(2)	0.3(1)		$33/2^+ \rightarrow 29/2^+$	$E2$
934.8(3)	1.7(2)	0.5(1)		$(33/2^+) \rightarrow 29/2^+$	$(E2)$
952.4(1)	8.6(5)	0.2(1)		$(39/2^-) \rightarrow (35/2^-)$	$(E2)$
965.0(1)	9.7(5)	4.1(2)	0.44(3)	$23/2^+ \rightarrow 21/2^-$	$E1$
967.2(1)	0.2(1)	0.5(1)		$17/2^+ \rightarrow 13/2^+$	$E2$
969.8(2)	1.0(1)	0.3(1)	0.56(19)[d]	$21/2^+ \rightarrow 19/2^-$	$E1$
990.9(1)	3.8(2)	2.7(1)	0.82(6)	$23/2^+ \rightarrow 21/2^+$	$M1/E2$
999.3(1)	10.7(7)	6.4(3)	0.77(9)	$19/2^+ \rightarrow 17/2^+$	$M1/E2$
1001.1(1)	63.0(3.6)	56.1(2.8)	0.51(1)	$15/2^- \rightarrow 13/2^+$	$E1$
1006.5(2)	1.7(2)	0.4(1)		$27/2^- \rightarrow 25/2^-$	$M1/E2$
1019.9(1)	2.0(2)	0.4(1)		$27/2^+ \rightarrow 25/2^+$	$M1/E2$
1021.4(2)		0.5(1)		$19/2^+ \rightarrow 15/2^+$	$E2$
1023.6(2)		0.8(1)		$(19/2^-) \rightarrow 15/2^-$	$(E2)$
1030.6(2)	3.6(3)	0.2(1)		$(45/2^+) \rightarrow (41/2^+)$	$(E2)$
1037.1(1)	6.1(4)			$(43/2^-) \rightarrow (39/2^-)$	$(E2)$
1038.7(1)		2.8(2)	0.76(10)	$15/2^+ \rightarrow 13/2^+$	$M1/E2$
1048.4(2)	3.3(2)	0.7(1)		$31/2^+ \rightarrow 27/2^+$	$E2$
1060.5(1)	6.1(4)	7.3(4)	1.05(5)	$17/2^+ \rightarrow 13/2^+$	$E2$
1075.3(1)		1.0(1)		$13/2^+ \rightarrow 11/2^+$	$M1/E2$
1080.4(1)	4.0(7)	0.8(1)	0.39(6)	$31/2^+ \rightarrow 29/2^+$	$M1/E2$
1081.3(2)	2.9(2)	0.4(1)		$(33/2^+) \rightarrow 29/2^+$	$(E2)$
1082.3(1)	3.2(6)	2.1(1)	0.93(13)[d]	$13/2^- \rightarrow 11/2^+$	$E1$
1084.9(2)		0.6(1)		$(23/2^+) \rightarrow 19/2^+$	$(E2)$
1095.0(2)	2.9(2)	0.2(1)		$(33/2^+) \rightarrow 29/2^+$	$(E2)$
1101.7(2)		1.1(1)		$5/2^+ \rightarrow 9/2^+$	$E2$
1103.7(1)	0.3(3)	0.8(1)		$19/2^+ \rightarrow 17/2^+$	$M1/E2$
1108.3(2)	4.7(3)			$(47/2^-) \rightarrow (43/2^-)$	$(E2)$
1127.0(1)	8.7(5)	3.5(2)	0.95(11)	$21/2^+ \rightarrow 17/2^+$	$E2$
1127.4(1)		1.2(1)	1.30(28)	$21/2^+ \rightarrow 19/2^+$	$M1/E2$
1152.7(1)	5.8(4)	0.9(1)		$(37/2^+) \rightarrow (33/2^+)$	$(E2)$

TABLE I. (*Continued*).

E_γ (keV)	$I_{\gamma,\text{thin}}$[a] (%)	$I_{\gamma,\text{backed}}$[b] (%)	DCO Ratio[c]	$I_i^\pi \rightarrow I_f^\pi$	Multipolarity
1152.9(1)	20.5(1.6)	13.6(7)	1.08(11)	$11/2^+ \rightarrow 9/2^+$	$M1/E2$
1166.7(3)	2.7(2)	0.1(1)		$(37/2^+) \rightarrow (33/2^+)$	$(E2)$
1190.8(2)	0.6(1)	0.3(1)		$21/2^+ \rightarrow 19/2^+$	$M1/E2$
1200.8(1)	0.3(1)	0.6(1)		$17/2^+ \rightarrow 15/2^+$	$M1/E2$
1205.6(2)	2.0(3)			$(43/2^+) \rightarrow (39/2^+)$	$(E2)$
1206.1(2)	4.0(3)			$(51/2^-) \rightarrow (47/2^-)$	$(E2)$
1219.1(3)	2.2(3)			$(49/2^+) \rightarrow (45/2^+)$	$(E2)$
1224.1(1)	5.4(3)	1.0(1)	1.45(38)[d]	$27/2^+ \rightarrow 23/2^+$	$E2$
1254.8(1)	4.0(7)	0.9(1)	1.56(37)[d]	$29/2^+ \rightarrow 25/2^+$	$E2$
1286.7(3)		0.3(1)		$15/2^+ \rightarrow 11/2^+$	$E2$
1291.4(2)	3.7(3)			$(41/2^+) \rightarrow (37/2^+)$	$(E2)$
1306.4(1)	1.0(1.0)	0.8(1)	0.43(11)	$15/2^+ \rightarrow 13/2^+$	$M1/E2$
1310.5(2)	3.0(3)			$(55/2^-) \rightarrow (51/2^-)$	$(E2)$
1347.8(1)		1.1(1)	1.13(22)	$15/2^+ \rightarrow 13/2^+$	$M1/E2$
1371.3(2)	0.6(2)	0.5(1)		$15/2^+ \rightarrow 13/2^+$	$M1/E2$
1378.1(4)	2.0(3)			$(59/2^-) \rightarrow (55/2^-)$	$(E2)$
1383.3(1)	1.9(3)	0.6(1)	1.96(28)[d]	$25/2^- \rightarrow 21/2^-$	$E2$
1392.8(1)	3.4(6)	4.0(2)	0.90(6)	$25/2^+ \rightarrow 21/2^+$	$E2$
1401.2(1)	$\equiv$100.0(7.6)	$\equiv$100.0(5.2)	1.05(3)	$13/2^+ \rightarrow 9/2^+$	$E2$
1425.2(2)	1.1(3)	0.9(1)		$17/2^+ \rightarrow 13/2^+$	$E2$
1435.4(5)	1.7(7)			$(53/2^+) \rightarrow (49/2^+)$	$(E2)$
1447.0(7)	1.0(3)			$(63/2^-) \rightarrow (59/2^-)$	$(E2)$
1448.7(1)	2.3(3)	1.3(1)	2.41(47)[d]	$27/2^- \rightarrow 23/2^-$	$E2$
1451.4(1)	2.3(2)	0.7(1)	1.69(71)[d]	$29/2^- \rightarrow 25/2^-$	$E2$
1466.2(2)	2.1(2)	0.8(1)	2.21(41)[d]	$19/2^+ \rightarrow 15/2^+$	$E2$
1500.5(1)	4.0(4)	1.9(1)	0.97(7)	$7/2^+ \rightarrow 9/2^+$	$M1/E2$
1518.3(1)		0.8(1)	1.10(15)	$15/2^+ \rightarrow 13/2^+$	$M1/E2$
1596.0(1)		0.5(1)		$15/2^+ \rightarrow 11/2^+$	$E2$
1619.4(2)		0.3(1)		$15/2^+ \rightarrow 11/2^+$	$E2$
1634.5(6)	1.2(3)			$(57/2^+) \rightarrow (53/2^+)$	$(E2)$
1638.2(3)		0.7(1)		$17/2^+ \rightarrow 13/2^+$	$E2$
1753.2(4)		0.2(1)		$9/2^+ \rightarrow (9/2^+)$	$(M1/E2)$
1767.1(2)		0.2(1)		$15/2^+ \rightarrow 11/2^+$	$E2$

[a]Relative coincidence intensities from thin-target data, corrected for detector efficiency and normalized to 100% for the 1401-keV transition.
[b]Relative coincidence intensities from backed-target data, corrected for detector efficiency and normalized to 100% for the 1401-keV transition.
[c]DCO ratios are from backed target data only and from gates on stretched $E2$ transitions, except where indicated otherwise.
[d]DCO ratio from gate on pure dipole transition.
[e]DCO ratio is for a peak composed of more than one transition.

stretched $E2$ transitions, and 0.50 for a pure stretched dipole transition. Note that a pure nonstretched dipole transition ($\Delta I=0$) would also be expected to have a DCO ratio of approximately 1.0.

The levels are arranged into a number of γ-ray cascades labeled 1 through 12, as shown in Fig. 2. For simplicity, they are all referred to as bands, although some cascades may not correspond to collective rotation. The left side of the level scheme including bands 1 through 8, contains the positive-parity states while the right side including bands 9 through 12, shows the negative-parity states. Only those parts of the level scheme which particularly deserve justification are discussed below, proceeding sequentially through the band numbers.

The 861-, 798-, and 664-keV transitions between bands 2 and 3 have DCO ratios which are not consistent with a stretched quadrupole nature; hence, band 2 is assigned signature $+1/2$, opposite to that of band 3. DCO ratios of the intraband transitions are consistent with a stretched quadrupole nature up through the $29/2^+$ level. The adjacent placement of the 847-keV doublet transitions is based on the fact that a gate at 847 keV shows a peak at the same energy which fits the intensity profile of the rest of the band, i.e., it is stronger than the 765-keV transition but weaker than the 903-keV transition. The higher energy γ ray of the doublet is placed above the lower energy one because gates on γ rays above the doublet show a slightly higher peak centroid than gates on those below. This difference in centroid is probably

enhanced by the proposed feedout at the $(33/2^+)$ level, which is discussed in more detail below.

The intensity profile of band 2 is somewhat peculiar in that gates on the 903-keV and higher transitions in band 2 show that the portion of the band above the $29/2^+$ and/or $(33/2^+)$ levels is significantly more intense than the transitions below those levels. Specifically, these gates, after efficiency correction, show an 847-keV peak which is significantly more than twice as intense as the 765- and 689-keV peaks. The 847-keV doublet complicates the analysis, but a reasonable explanation can still be made. If it is assumed that the intensity loss occurs at one level, it would be at the $(33/2^+)$ level because, in the 1031-keV gate, the peak at 847 keV is not nearly twice as intense as that at 903 keV, meaning that the full flux of the 903-keV transition passes through the upper transition of the doublet, but not all of it goes through the lower one. From the 1031-keV gate, the intensity of the peak at 847 keV is within statistical error of the sum of the intensities of the peaks at 903 keV (through the upper transition of the doublet) and 765 keV (passing through the lower transition). A similar argument can be made using the 903-keV gate. The measured intensities indicate that about half the flux of the band is lost at the $(33/2^+)$ state, as indicated in Fig. 2. Unfortunately, no other discrete transitions from this level could be found, perhaps because the flux is divided over several weaker transitions or because the energy of the transition is so high that low detector efficiency precludes its observation.

The spin and parity assignment of the 1501-keV level of band 3 is critical to the determination of the configuration of the rotational band built upon it. Previous work based on γ-ray angular distributions and decay characteristics [22] assigned it to be $7/2^+$ or $9/2^+$. This was confirmed by analysis of the deuteron spectrum from the ^{110}Cd(^{3}He,d) reaction, which indicated an $l=4$ angular momentum transfer [24]. The presence of the 1619-keV transition out of the $15/2^+$ member of band 3 to the $11/2^+$ state at 1153 keV effectively rules out the possibility that the bandhead spin is $9/2^+$; since the DCO ratios of the 532- and 740-keV transitions of band 3 are consistent with a stretched quadrupole nature, a $9/2^+$ bandhead spin assignment would imply an $M3$ character for the 1619-keV transition. Hence, band 3 is assigned a $7/2^+$ bandhead corresponding to a signature of $-1/2$. This $7/2^+$ assignment requires that the 1501-keV transition to the ground state have an $M1/E2$ character in order to be consistent with its DCO ratio.

The near degeneracy of the $(33/2^+)$ levels in band 5 and band 8 (14 keV difference) indicates a rather small interaction matrix element between the two states of $\lesssim 7$ keV (half the level difference). Thus, the unusually large feeding from band 5 into band 8 via the 560-keV transition, which suggests that the $(33/2^+)$ levels are strongly mixed, is the result of an ''accidental'' degeneracy and does not reflect any similarity in structure. Of the nearly degenerate pair of levels, the level at higher energy is placed in band 5 because of the greater branching to it from the $(37/2^+)$ level of the band.

One unusual aspect of the level scheme deserves particular attention. In the course of the analysis of band 9, a discrepancy in excitation energy of 5 keV was discovered. This was traced to a previously overlooked level (at 2619 keV) which is above but nearly degenerate with the $17/2^-$ level (at 2614 keV) which decays via the intense 212-keV transition. The levels are connected by a 5-keV transition, through which almost all of the flux of band 9 passes with little or no observed hindrance. Although this may seem unlikely due to the low transition energy, the Weisskopf estimate for an $M1$ transition of this energy including electron conversion predicts a half-life of the order of 1 ns. This lifetime is sufficiently short that the observation of coincidences between transitions above and below the level would not be significantly suppressed by the experimental time window. The existence of the weak 129-keV crossover transition as well as numerous γ-ray energy sums involving the firmly established bands 8 and 12 confirm the existence of the two levels.

The spin and parity assignment of the upper level at 2619 keV is based on the following observations. The lower level at 2614 keV has been assigned $17/2^-$. States in band 9 above this level are almost certainly also of negative parity in keeping with its bandlike structure and the systematics of neighboring odd-mass In isotopes [27]. The possibility that the transition is an $I \rightarrow I$ $M1/E2$ transition, with both levels having spin $17/2^-$, is unlikely for several reasons. Since bands 8 and 9 have opposite parity, only transitions with $\Delta I=1$ or 0 will be observed between them, making the spin of the 2619-keV level at least 19/2, assuming the spin assignments of band 8 are correct. In addition, the wave functions of the two levels appear to be very distinct and unmixed, since transitions from higher levels greatly favor one state over the other; e.g., decay from the next higher level of band 9 (at 2743 keV) greatly favors the upper of the two levels via the 123-keV transition over the lower level via the 129-keV transition. If the two levels had the same spin, this would be very difficult to explain, as it would require exceedingly pure and orthogonal wave functions to achieve an interaction matrix element of $\lesssim 3$ keV. Also, the $M1$ decay from a $17/2^-$ 2619 keV level would greatly favor a 217-keV transition to the 2402-keV $15/2^-$ level over the 5-keV $M1$ transition, but the data show no evidence for such a transition. Stretched $E2$ character for the transition is also ruled out by the presence of the 129-keV transition as well as by the greatly suppressed transition rate expected at 5 keV. The only reasonable possibility is a $\Delta I=1$ $M1$ transition, giving a spin and parity of $19/2^-$ for the level.

Band 10 could not be linked to lower spin states; its decay pattern is indicated in Fig. 2 by dashed arrows, and its excitation energy and spin-parity assignments have been estimated by intensity and feeding considerations. Intraband transitions are assumed to be stretched dipoles because quadrupoles would make the band far more yrast than the rest of the scheme, in contradiction to its limited extent and relatively modest intensity.

The analysis of band 11 was reported in the first publication from this collaboration [17], which also discusses the high-spin DSAM lifetime data from the present series of experiments. For band 11, the DSAM analysis was carried out by the centroid shift method and the data were consistent with a constant in-band quadrupole moment of $Q_0=2.3(3)$ eb, corresponding to an axial prolate deformation of $\beta_2=0.18(2)$. Unfortunately, due to insufficient statistics and contamination of the γ-ray lines, lifetime information could not be reliably extracted for other structures.

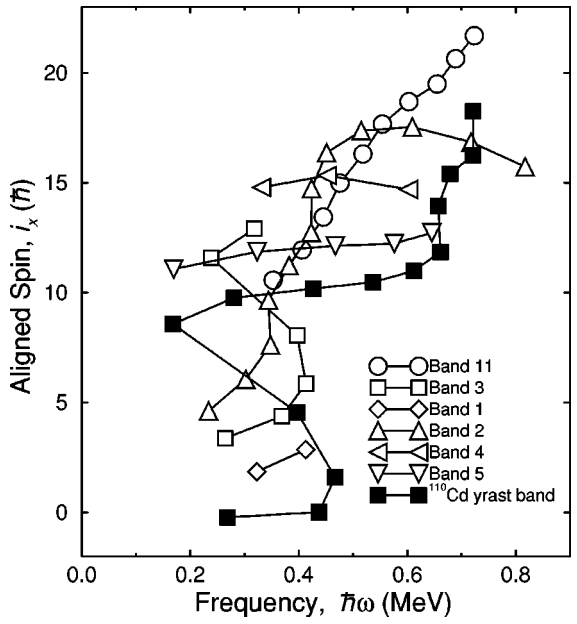

FIG. 3. Experimental aligned spins as a function of rotational frequency for the $\Delta I=2$ bands established in ^{111}In and the yrast band in ^{110}Cd [14], relative to a Harris parametrization of the core of $\mathcal{J}_0=5.0\hbar^2/\mathrm{MeV}$ and $\mathcal{J}_1=15.0\hbar^4/\mathrm{MeV}^3$.

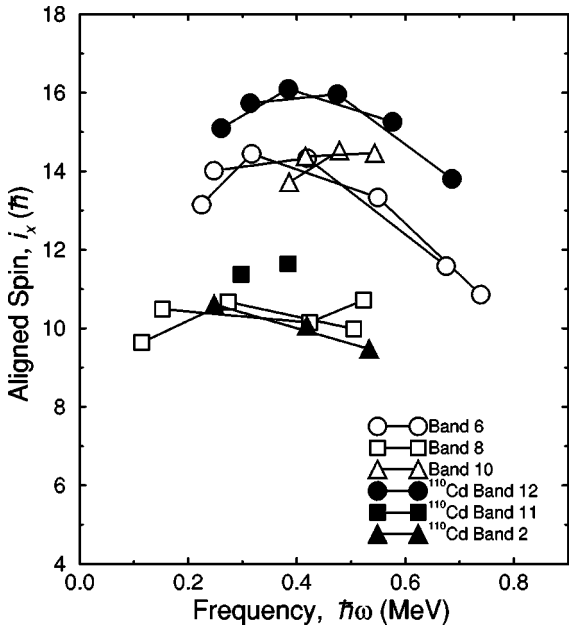

FIG. 4. Experimental aligned spins as a function of rotational frequency for the $\Delta I=1$ bands 6, 8, and 10 in ^{111}In and the related bands 12, 11, and 2 in ^{110}Cd [14], relative to a Harris parametrization of the core of $\mathcal{J}_0=5.0\hbar^2/\mathrm{MeV}$ and $\mathcal{J}_1=15.0\hbar^4/\mathrm{MeV}^3$.

Despite extensive attempts using the backed-target data to find discrete transitions linking band 11 to states of known excitation energy, it could not be definitively connected and consequently the spin and parity assignment remain tentative and the excitation energy is estimated. The pattern by which the band feeds into the lower-lying states is indicated by dashed arrows in Fig. 2.

IV. DISCUSSION

For completeness, all levels identified with ^{111}In in the analysis of the present data are presented in Fig. 2 and Table I. Figures 3 and 4 contain the experimental aligned spins as a function of rotational frequency for the observed band structure. With the exception of a brief overview of the current understanding of the low-spin states of the nucleus, the following discussion will focus on those structures thought to involve at least modest deformation which can be interpreted in terms of rotational or quasi-rotational characteristics. The structures of states belonging to many of the irregular structures observed at high spin involve multiple single-particle configurations in a spherical potential and clearly cannot be understood within this framework.

The low-spin level structure of ^{111}In has been the subject of several previous experiments employing beams of protons [21,22,25], deuterons [20], α particles [23], and ^{3}He [24]. The resulting interpretations of the observed states, with the exception of four putatively deformed states to be discussed later in connection with band 3, involve spherical single-particle or vibrational characteristics. The structure of those states which have been observed in the present data can be summarized in a general way as follows. The $9/2^+$ ground state is associated with the $\pi g_{9/2}$ hole orbital. The $11/2^+$ and $13/2^+$ states of band 7 are members of the multiplet of states formed from coupling the proton $g_{9/2}$ hole to the 2^+ vibrationlike state of ^{112}Sn [23,25]. Similarly, the $15/2^+$ and $17/2^+$ states of band 7 can be associated with the $\pi g_{9/2}^{-1}\otimes 4^+$ multiplet. The $21/2^+$ level is an isomer with a 13.7(4) ns half-life [27] which is related to the 6^+ isomer in the ^{112}Sn core and corresponds to the $g_{9/2}$ proton hole coupled to a two-quasineutron state of predominantly $d_{5/2}g_{7/2}$ character [23]. The negative-parity levels of bands 9 and 12 can similarly be viewed as a $g_{9/2}$ proton hole coupled to the low-lying negative-parity states of ^{112}Sn which involve two-quasiparticle neutron excitations, including to some extent neutron $d_{5/2}h_{11/2}$ octupole correlations [28,29].

A. Decoupled bands

As discussed in Sec. I, decoupled bands in indium nuclei almost certainly result from $1p$-$1h$ proton excitations from the $g_{9/2}$ orbital to one of the $g_{7/2}$, $d_{5/2}$, or $h_{11/2}$ orbitals above the shell gap. These $1p2h$ configurations are believed to be involved in the configurations of bands 11, 3, 1, 2, 4, and 5, which are discussed below in that order.

1. Band 11

Band 11 is the most intense decoupled band and extends to the highest spin. It is interpreted as a rotational band built on the $1p$-$1h$ proton excitation from the $\pi g_{9/2}$ to the $\pi h_{11/2}$ orbital, i.e., the $1p2h$ $\pi h_{11/2}g_{9/2}^{-2}$ configuration, as discussed in the initial report of this work [17]. Although it could not be firmly linked to states of known spin and parity, it feeds negative-parity states only and thus is most likely also of negative parity. The gradual increase in aligned spin, apparent in Fig. 3, and the $\mathcal{J}^{(2)}$ dynamic moment of inertia (not shown) are very similar to those of the $\pi h_{11/2}$ intruder band in the ^{113}Sb isotone, which is based on a $3p2h$ $\pi h_{11/2}g_{7/2}^2g_{9/2}^{-2}$ configuration. In that nucleus, the smooth increase in aligned spin is attributed to a strong proton-neutron

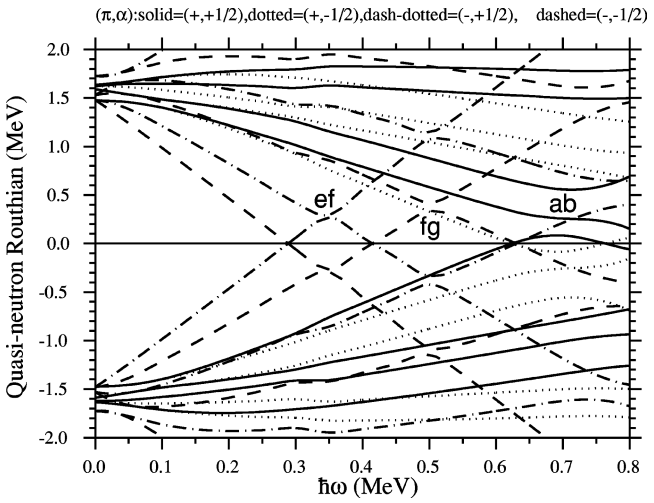

FIG. 5. Quasineutron Routhians for ^{111}In as a function of rotational frequency, calculated using the cranked shell model with a Woods-Saxon potential. The deformation was specified by the parameters $\beta_2=0.15$, $\beta_4=0.00$, and $\gamma=3°$, and the pairing was fixed at the BCS value. The labels ef, fg, and ab indicate the first two crossings of negative-parity neutrons and the first positive-parity neutron crossing, respectively.

interaction between the $h_{11/2}$ proton and the aligning $h_{11/2}$ neutrons [6]. This may explain why a standard cranked shell model (CSM) calculation, which does not properly account for this residual interaction, incorrectly predicts a sharp increase in aligned spin at a well-defined frequency due to $h_{11/2}$ neutron pair alignment. A CSM calculation appropriate for ^{111}In is displayed in Fig. 5; the predicted neutron alignment frequency is defined by the crossing labeled ef. The DSAM lifetime data are consistent with a constant in-band quadrupole moment of 2.3(3) eb, corresponding to a quadrupole deformation of $\beta_2=0.18(2)$ if axial symmetry is assumed. This deformation is consistent with total Routhian surface (TRS) calculations [30] for the $(\pi,\alpha)=(-,-1/2)$ configuration.

Additional support for this interpretation can be found in recent theoretical work using an extended TRS model [16]. In addition to the standard TRS model, a quadrupole pairing interaction was used to better account for particle-particle correlations, and a new method was employed which approximately restores the particle number symmetry in order to avoid pairing difficulties near closed shells. These pairing-deformation self-consistent TRS calculations, which involve no free parameters, were performed for the proposed configuration of band 11 in ^{111}In and give excellent agreement with the data [16]; although the deformation is somewhat overpredicted compared to the value determined by the present DSAM measurements, the smooth increase in angular momentum of the band is reproduced to within about $1\hbar$ across the entire observed frequency range. The agreement between these calculations and experiment is also reasonable for the yrast bands in even-mass Cd and Te nuclei, and in odd-mass Sb nuclei [16], and is in any case a significant improvement over the standard calculations.

2. Bands 3 and 1

Band 3 has firm spin and parity assignments and also appears to be rotational in character. Given its positive parity and signature of $-1/2$, band 3 is most likely based on the $1p$-$1h$ proton excitation into the $\pi g_{7/2}$ orbital, or the $1p2h$ $\pi g_{7/2}g_{9/2}^{-2}$ configuration. In Fig. 3, a sharp backbend is evident at 0.35 MeV/$\hbar$ with a gain in aligned spin of roughly $9\hbar$. Compared to band 11, it is expected that the standard CSM would better reproduce the behavior of the aligned spin of band 3 because the occupied proton intruder orbital ($g_{7/2}$) is not in the same shell as the quasiparticle pair expected to align first ($h_{11/2}$ neutrons) and hence the effect of the proton-neutron interaction is less significant. For the calculations, the measured quadrupole moment of band 11 provides a reasonable estimate for the deformations of all the $1p2h$ configurations of this nucleus, although the actual deformations of configurations involving the less deformation-driving positive parity intruder orbitals may be slightly smaller. CSM calculations have been performed for a range of deformations around this estimate; the ef crossing in the calculation at a quadrupole deformation of $\beta_2=0.15$, shown in Fig. 5, accurately reproduces the crossing frequency, the gain in aligned spin, and the small interaction strength of the observed backbend.

It is interesting to compare the aligned spin of band 3 as a function of rotational frequency to that of the yrast band in the ^{110}Cd core which is of almost purely $2h$ character [14]. In Fig. 3, it is seen that the magnitude of the aligned spins of ^{111}In is very nearly 3.5 $\hbar$ greater than that of the ^{110}Cd core over the entire observed frequency range, as expected from the placement of the odd proton in the low-Ω $g_{7/2}$ orbit. The backbends in both bands occur at essentially the same frequency and with similar interaction strengths and gains in aligned spin, consistent with $h_{11/2}$ neutron pair alignment. This implies a similar deformation for the ^{110}Cd yrast band, which is consistent with lifetime measurements in that nucleus [31]. If the deformation assumptions presented above are correct, it is somewhat surprising that the additional occupation of a deformation-driving intruder orbital in the ^{111}In case does not influence the deformation more strongly.

Although prior to this work, rotational bands had never been observed in ^{111}In, it must be noted that the deformed nature of the $7/2^+$ bandhead of band 3 had been suggested in several previous works [22,24,25]. These studies suggested that low-lying $1/2^+$, $3/2^+$, $5/2^+$, and $7/2^+$ states at 1188, 1345, 1102, and 1500 keV, respectively, belong to a rotational sequence based mainly on the [431]$1/2^+$ Nilsson orbital, for the following reasons. The low energy of the $1/2^+$ and $3/2^+$ states could not be explained by a $g_{9/2}$ hole coupled to the Sn core because it would require coupling to the higher-lying 4^+ state of the core. The $5/2^+$ and $7/2^+$ states appear to be of predominantly $1p2h$ rather than $1h$ nature, because both are strongly populated in proton transfer reactions on Cd nuclei, but not in proton stripping reactions on Sn nuclei [24]. The particle rather than hole nature of the $7/2^+$ state is further supported by a recent work [25] which ruled out the possibility that the state is a member of the $g_{9/2}^{-1}\otimes 2_1^+$ multiplet because a nearby $7/2^+$ state at 1543-keV (unobserved in the present experiments) was identified with that multiplet based on analyses of DSAM lifetime measurements and IBFM calculations. In addition, the rotational interpretation was supported by early Nilsson band-head cal-

culations for neighboring isotopes [32] which predicted a deformed minimum at low energies. However, the ordering of the states was difficult to reproduce in calculations [24], and again, no rotational γ-ray cascades were observed. The present data show no evidence for either the $1/2^+$ or $3/2^+$ states, and the $5/2^+$ and $7/2^+$ states appear to belong to different γ-ray cascades, with only the $7/2^+$ level leading to an extended rotational band, band 3.

In light of these arguments, the $5/2^+$ state of band 1 at 1102 keV may then be viewed as an intruder $1p2h$ state of predominantly $\pi d_{5/2}$ character. Indeed, the $(9/2^+)$ and $(13/2^+)$ levels of band 1 could belong to a rotational band built on this state. Since the $\pi g_{7/2}$ and $\pi d_{5/2}$ orbitals are nearly degenerate and are strongly mixed at the deformations appropriate for this nucleus, some mixing with the unfavored signature of the $g_{7/2}$ orbital is expected. The aligned spin for band 1 is also displayed in Fig. 3, but because of its limited extent, the detailed rotational characteristics of the band cannot be analyzed further.

3. Band 2

Band 2 presents several difficulties in its interpretation. It decays into band 3 at frequencies below that of the $\nu h_{11/2}$ pair alignment, and extends to much higher spin. In this nucleus, the configuration most likely responsible for a positive-parity intruder band at high spin is that involving a p-h excitation into the $\pi g_{7/2}$ orbital, i.e., the configuration of band 3. In the cranking picture, this should be favored over the $\pi d_{5/2}$ excitation because the configuration with a larger expectation value for j_x is lowered more in energy with increasing frequency due to the $-\omega j_x$ term in the cranking Hamiltonian. However, the proposed spins of band 2 give it signature $+1/2$ which is consistent with the unfavored signature of the $g_{7/2}$ orbital, or the favored signature of the $d_{5/2}$ orbital, or a mixing of these two configurations. At lower spins, band 2 may indeed correspond mainly to the opposite (unfavored) signature of the configuration of band 3 as it clearly lies at higher energy than band 3. At higher spins, however, it is difficult to explain why it continues to be observed and band 3 does not. If band 2 were associated with the $\pi d_{5/2}$ orbital, it is unusual that it does not decay into band 1 which is also believed to involve the $\pi d_{5/2}$ excitation, and that the favored band based on the $g_{7/2}$ proton excitation is not also observed at high spins.

In Fig. 3, two increases in the aligned spin of band 2 are observed, at 0.35 and 0.42 MeV/$\hbar$. The first could be associated with $\nu h_{11/2}$ alignment, but the gain in aligned spin is considerably smaller than expected. The frequency of the second increase in aligned spin cannot be reproduced by the CSM to within 0.05 MeV/$\hbar$, using a wide range of parameters (β_2 values from 0.12 to 0.30 and γ values from $-30°$ to $+30°$). This may be related to the loss of intensity via an unidentifiable path at the $(33/2^+)$ level, described earlier in Sec. III. What appears to be the second alignment may instead be a crossing with another band based on a substantially different configuration. If this were the case, the $(33/2^+)$ state could be the lowest observed state of the new band, and its decay might be expected to fragment over many paths, only one of which (the lower 847-keV transition to the $29/2^+$ state of band 2) is identified. The configuration of such a band could involve an additional positive-parity two-quasineutron excitation to account for its large aligned spin. Another possibility is that the lower 847-keV transition is actually a member of the lower band, and that the partial decay from the upper band to the lower band is itself fragmented and hence not observed. In this case, the upper band might have spins different from those suggested, and thus might be consistent with the favored signature of the expected intruder configuration after all, although the lack of a decay path to band 3 would be difficult to explain. Greater experimental sensitivity in this region of the band is required to resolve these ambiguities.

4. Bands 4 and 5

Bands 4 and 5 are somewhat weak and poorly developed. To the extent that these structures may be interpreted as rotational bands, they are most likely related to the $1p2h$ intruder configurations of bands 2 and 3, but with different neutron excitations. The aligned spins are large, as seen in Fig. 3, most likely due to the presence of aligned $h_{11/2}$ neutrons. Band 4 has about 3 $\hbar$ more aligned spin than band 5, and the experimental Routhian of band 4 crosses that of band 5 at about 0.6 MeV/$\hbar$. This crossing frequency and difference in aligned spin could be attributed to midshell $g_{7/2}(d_{5/2})$ neutron alignment. In the CSM calculations shown in Fig. 5 which are made at a quadrupole deformation of $\beta_2=0.15$, the ab neutron crossing occurs at about 0.7 MeV/$\hbar$, but this value reduces to 0.65 MeV/$\hbar$ at $\beta_2=0.12$. Since the vacuum proton configuration would result in two bands with no signature splitting, the proton configurations of bands 4 and 5 most likely include the proton p-h excitation into the $g_{7/2}$ or $d_{5/2}$ orbitals. Indeed the 12 $\hbar$ of aligned spin of band 5 can be accounted for by about 10 $\hbar$ expected from aligned $h_{11/2}$ neutrons and 2 to 3 $\hbar$ from the low-Ω intruder orbitals.

5. Smooth band termination calculations

Smooth band termination calculations have been performed for ^{111}In [33], but the conditions for the observation of this phenomenon have not proved to be favorable and comparisons with the present experimental results are not particularly meaningful. Because the existing calculations do not include pairing [10] and yet pairing is expected to play a significant role in the band structure up to spins of about 20 $\hbar$, only bands 2 and 11 might be considered reasonable candidates. Of these, only band 2 exhibits the characteristic decrease in $\mathcal{J}^{(2)}$ dynamic moment of inertia as the highest spins are approached. Indeed, band 2 shows some similarities to the calculation for the $\pi g_{7/2} g_{9/2}^{-2} \otimes \nu h_{11/2}^4$ configuration; however, the experimental ambiguities concerning the high-spin region of band 2, discussed earlier, make comparisons with theory difficult. Moreover, because of the large number of valence neutrons, the terminating spins expected for the intruder configurations are near 40 $\hbar$, considerably beyond the highest spins observed in these experiments. The best agreement between the smooth band termination calculations and experiment has generally been obtained for the more neutron-deficient nuclei with $N \leqslant 60$.

B. High-*K* bands

In contrast to the relatively straightforward interpretations of the decoupled bands in ^{111}In, there are several high-*K*

configurations on which strongly-coupled bands in this nucleus might be based. The configurations expected to have the largest deformation involve the $2p$-$2h$ proton excitation responsible for the well-deformed intruder bands in the Sn, Sb, and Te nuclei. A band based on such a $2p3h$ configuration in ^{111}In should be even more deformed than the $1p2h$ decoupled bands already discussed. Less deformed high-K bands might involve $1p$-$1h$ proton excitations, or $1p2h$ proton configurations, in which the large K value results from either a two-quasineutron excitation or the coupling of the two $g_{9/2}$ proton holes to 8^+. Lastly, configurations involving no p-h excitations may be observed in which only neutron excitations are responsible for inducing deformation. It is plausible that these configurations involve some deformation, because the $2h$ configurations of neighboring even-mass Cd nuclei have been found to achieve moderate deformation from neutron excitations alone [34,31].

In ^{111}In, the high-K strongly coupled bands 6, 8, and 10 appear somewhat rotational in character, but do not have the characteristics of well-deformed rotors. The level spacings are often irregular, and only a few $E2$ crossover transitions are observed, suggesting relatively low $B(E2)$ strengths and consequently only modest deformations at best. In addition, these bands exist over a limited range of angular momentum of only $5-8\ \hbar$. These qualitative observations all but rule out the involvement of $2p$-$2h$ excitations in the configurations of these bands, and render doubtful the possibility that even $1p$-$1h$ excitations are involved.

1. Bands 6 and 8

High-K bands of this nature have some precedent in this region, most notably in the ^{110}Cd core [14] in which two bands have very similar characteristics to bands 6 and 8 in ^{111}In. Specifically, bands 6 and 8 appear to be closely related to the bands labeled 12 and 11, respectively, in Ref. [14]. Band 6 feeds into band 8 in ^{111}In just as band 12 feeds into band 11 in ^{110}Cd, and the aligned spins, compared in Fig. 4, are also very similar, but about $1-2\ \hbar$ lower in ^{111}In for both cases.

It is interesting that the differences between the properties of the In and Cd bands just discussed can be simply explained as the effect of adding a $g_{9/2}$ proton to the proposed configurations of the related Cd bands. The ^{110}Cd band 11 has been associated with the $\pi[g_{9/2}^{-2}]_{8^+}\otimes\nu h_{11/2}^2$ configuration, and band 12 with the same configuration coupled to an aligned $g_{7/2}$ neutron pair [14]. Assuming these proposed configurations are correct, the lowest energy orbital available to the extra proton in ^{111}In is $g_{9/2}$, which would only complete a pair with one of the previous unpaired $g_{9/2}$ protons (all Ω orbits contain at least one proton), resulting in the $g_{9/2}^{-1}$ ground-state proton configuration coupled to the same neutron configurations. Although this configuration might be expected to be less deformation-driving than the alternative $\pi g_{7/2}[g_{9/2}^{-2}]_{8^+}$ configuration involving a $1p$-$1h$ proton excitation, it is more consistent in several respects. First, the bandhead spins in ^{111}In are expected to be about $3\ \hbar$ smaller than in ^{110}Cd due to the completion of the lower $\Omega=7/2$ $g_{9/2}$ proton pair, and this is indeed the case. Bands 8 and 6 in ^{111}In begin at spins of 9.5 and 13.5 $\hbar$, respectively, compared to 14 and 17 $\hbar$ for bands 11 and 12 in ^{110}Cd. Second, the aligned spins are expected to be only slightly smaller in ^{111}In due to the loss of the small aligned spin contribution of the high-Ω $g_{9/2}$ hole filled by the odd proton, and this is also the case, as shown in Fig. 4. Finally, the ^{110}Cd bands are about 3 MeV higher in excitation energy, roughly what is expected for the energy required to break a pair and promote a $g_{9/2}$ proton to the next available substate (in ^{111}In, the $\pi g_{9/2}^{-1}$ configuration is the proton vacuum state and obviously requires no excitation energy). If the odd proton were instead excited into an orbital above the shell gap, these quantities would be expected to compare very differently; in ^{111}In, the bandhead spins and aligned spin would be larger rather than smaller than those in ^{110}Cd (due to the large aligned spin of the low-Ω orbitals above the gap), and the excitation energy difference between the ^{110}Cd and ^{111}In bands would be smaller due to the energy required for the p-h excitation of the odd proton in the In case.

There are, however, some difficulties with the interpretation of these structures as conventional rotational bands based on the proposed configurations. First, if the differences between bands 6 and 8 in ^{111}In and between bands 11 and 12 in ^{110}Cd are attributed to aligned $g_{7/2}$ neutrons, the standard CSM incorrectly predicts the crossing frequency. The experimental Routhians of bands 8 and 6 in ^{111}In and of bands 11 and 12 in ^{110}Cd cross at frequencies of 0.43 and 0.39 MeV/$\hbar$, respectively, but the CSM predicts the ab alignment to occur above 0.60 MeV/$\hbar$ in each case. Second, the deformations associated with the proposed configurations are expected to be quite small; the $\pi g_{9/2}^{-1}$ ground state in ^{111}In is spherical as is the $\pi[g_{9/2}^{-2}]_{8^+}$ state in ^{110}Cd (no bands are built on these states). Lastly, the $B(M1;I\rightarrow I-1)/B(E2;I\rightarrow I-2)$ ratios of reduced transition probabilities in these bands tend to be very large. For most of the levels in these bands, $E2$ crossover transitions are not observed, but minimum $B(M1)/B(E2)$ ratios can be determined from reasonable estimates of the maximum $E2$ intensity consistent with the background at their expected energies. The $B(M1)/B(E2)$ ratios for most of the band members are at least $50-100\ (\mu_N/e\mathrm{b})^2$. Quantitative ratios can only be extracted for the top three levels of band 8 due to the observation of $E2$ crossovers from these levels, and they show an unexpected rapid decrease at the top of the band, changing from 70(11) to 34(3) to 20(2) $(\mu_N/e\mathrm{b})^2$ for the $29/2^+$, $31/2^+$, and $(33/2^+)$ levels, respectively.

2. Magnetic rotation interpretation

Some of the unusual features of these bands are shared by the so-called dipole bands in the Pb region [35], which have been recently interpreted with considerable success in terms of a phenomenon called ''magnetic rotation'' [36]. Magnetic rotation is expected to occur in nuclei in which the valence configurations involve high-j particles and holes of protons in one case and neutrons in the other. This is just the case with In and Cd nuclei which have a proton hole(s) in the $g_{9/2}$ shell and neutron particles in the $h_{11/2}$ shell near the Fermi surface. The qualitative features of the In and Cd bands just discussed can be explained within the magnetic rotation framework.

At a spherical shape, the energetically preferred orientation for the coupling of the spins of the valence proton holes and neutron particles is a perpendicular one because this maximizes the spatial overlap of the occupied orbitals resulting in increased binding due to the attractive residual interaction. However, in these particular nuclei with few proton holes and neutron particles, this orientation persists and is indeed further lowered in energy at a nonzero quadrupole deformation (ignoring for the moment the energy required to deform the core), which breaks the spherical degeneracy of the various Ω substates leaving the holes in high-Ω orbitals and the particles in low-Ω orbitals. This coupling results in a significant angle between the total angular momentum vector and the symmetry axis of the core. Thus, the detailed model which accounts for magnetic rotation, the tilted axis cranking (TAC) model [37], is essentially a generalization of the standard CSM in which cranking around an axis which is not necessarily perpendicular to the symmetry axis of the nucleus is possible.

Because the two perpendicular components of the total spin are from different nucleons with very different g factors, the orientation of the magnetic moment deviates substantially from the total angular momentum axis. When the mean field is cranked about this axis, the significant component of the magnetic moment perpendicular to it gives rise to large $M1$ transition probabilities. The spin itself is generated by a gradual alignment of the proton and neutron spins along the direction of the total angular momentum. The resulting ''shears'' bands, named for the resemblance of their underlying structure to the closing of the blades of a pair of shears, are not expected to extend across a large spin range because there is a limited amount of angular momentum which can be generated from the alignment of the proton and neutron spins, although additional quasiparticle alignment may contribute more spin. Since the $B(E2)$ strength is small due to the weak quadrupole deformation and the $B(M1)$ strength is large due to the TAC mechanism, the $B(M1)/B(E2)$ ratios are usually so large in the lower-spin region of these bands that the $E2$ crossover transitions are not observed. However, as the proton and neutron spins align, the component of the total magnetic moment perpendicular to the total nuclear spin decreases, and the $M1$ transition probabilities will decrease. Since the quadrupole collectivity is not expected to change significantly, $B(M1)/B(E2)$ ratios will decrease with increasing spin in the band, and stretched $E2$ transitions may begin to compete with the $M1$ transitions. This effect can be seen at the top of band 8 in Fig. 2 and the decreasing experimental $B(M1)/B(E2)$ ratios quoted earlier qualitatively support this interpretation.

In a concurrent theoretical study, shell model calculations have been performed for several neutron-deficient odd-In nuclei including ^{111}In, to ascertain whether these nuclei indeed generate angular momentum in this special way [38]. The results indicate that magnetic rotation is an active mechanism in these nuclei, and for ^{111}In, fair agreement between bands 6 and 8 and calculated shears sequences involving their proposed configurations is obtained. This agreement in addition to the qualitative agreement just discussed, are strong arguments to associate bands 8 and 6 in ^{111}In, and thus also the related dipole bands in ^{110}Cd, with the magnetic rotation mechanism. Differences between the bands can be expected from different configurations of neutrons in the positive-parity $g_{7/2}$ and $d_{5/2}$ orbitals.

3. Band 10

The dipole band 10 may also be related to a similar structure in ^{110}Cd, labeled band 2 in Ref. [14], which is associated with the $\pi[g_{9/2}^{-2}]_{8^+} \otimes \nu h_{11/2} g_{7/2}(d_{5/2})$ configuration. In contrast to bands 8 and 6, band 10 is not consistent with coupling an additional $g_{9/2}$ proton to the configuration of the related ^{110}Cd band, because its excitation energy is about the same as or perhaps higher than that of band 2 in ^{110}Cd, and it also has a higher bandhead spin and larger aligned spins (the estimated spins and excitation energy of band 10 can be considered a lower limit based on feeding arguments). As discussed earlier, completing a proton pair with one of the unpaired $g_{9/2}$ protons in the ^{110}Cd configuration would result in lower excitation energy, bandhead spin, and aligned spins compared to the related Cd band. Therefore, band 10 may involve an additional aligned $g_{7/2}$ or $h_{11/2}$ neutron pair to make up the observed differences. In this case, band 10 would most likely also require a shears-type mechanism to generate its angular momentum. Alternatively, the extra proton in ^{111}In might occupy an orbital above the shell gap to account for the extra excitation energy and aligned spins. In this case, a larger deformation would be expected and the band might involve collective rotation to a greater degree. The lack of firm spins, parities, and excitation energy of the band preclude a more detailed analysis of this band.

V. CONCLUSIONS

A detailed level scheme for the ^{111}In nucleus has been constructed, exhibiting interesting collective as well as novel single particle excitations. Unambiguous evidence of proton p-h excitations is found for the first time in a $Z<50$ nucleus in the form of decoupled bands involving proton $g_{7/2}(d_{5/2})$ and $h_{11/2}$ orbitals above the $Z=50$ spherical shell gap. The ^{111}In nucleus also appears to be a favorable case for the observation of magnetic rotation which is manifest as high-spin $\Delta I=1$ bands with no signature splitting and large $B(M1)$ strengths, but only a small associated deformation.

ACKNOWLEDGMENTS

This work was supported in part by the U.S. National Science Foundation, the Natural Sciences Research Council of Canada, AECL Research, and the UK Engineering and Physical Sciences Research Council. We thank I. Ragnarsson and A. V. Afanasjev for providing smooth band termination calculations. We also thank the staffs of the SUNY Stony Brook and TASCC accelerator facilities.

[1] A. K. Gaigalas, R. E. Shroy, G. Schatz, and D. B. Fossan, Phys. Rev. Lett. **35**, 555 (1975).
[2] R. E. Shroy, A. K. Gaigalas, G. Schatz, and D. B. Fossan, Phys. Rev. C **19**, 1324 (1979).
[3] R. Wadsworth, C. W. Beausang, M. Cromaz, J. DeGraaf, T. E. Drake, D. B. Fossan, S. Flibotte, A. Galindo-Uribarri, K. Hauschild, I. M. Hibbert, G. Hackman, J. R. Hughes, V. P. Janzen, D. R. LaFosse, S. M. Mullins, E. S. Paul, D. C. Radford, H. Schnare, P. Vaska, D. Ward, J. N. Wilson, and I. Ragnarsson, Phys. Rev. C **53**, 2763 (1996).
[4] R. Wadsworth, H. R. Andrews, C. W. Beausang, R. M. Clark, J. DeGraaf, D. B. Fossan, A. Galindo-Uribarri, I. M. Hibbert, K. Hauschild, J. R. Hughes, V. P. Janzen, D. R. LaFosse, S. M. Mullins, E. S. Paul, L. Persson, S. Pilotte, D. C. Radford, H. Schnare, P. Vaska, D. Ward, J. N. Wilson, and I. Ragnarsson, Phys. Rev. C **50**, 483 (1994).
[5] D. R. LaFosse, D. B. Fossan, J. R. Hughes, Y. Liang, P. Vaska, M. P. Waring, J. y. Zhang, R. M. Clark, R. Wadsworth, S. A. Forbes, and E. S. Paul, Phys. Rev. C **51**, R2876 (1995).
[6] V. P. Janzen, H. R. Andrews, B. Haas, D. C. Radford, D. Ward, A. Omar, D. Prévost, M. Sawicki, P. Unrau, J. C. Waddington, T. E. Drake, A. Galindo-Uribarri, and R. Wyss, Phys. Rev. Lett. **70**, 1065 (1993).
[7] H. Schnare, D. R. LaFosse, D. B. Fossan, J. R. Hughes, P. Vaska, K. Hauschild, I. M. Hibbert, R. Wadsworth, V. P. Janzen, D. C. Radford, S. M. Mullins, C. W. Beausang, E. S. Paul, J. DeGraaf, I.-Y. Lee, A. O. Macchiavelli, A. V. Afanasjev, and I. Ragnarsson, Phys. Rev. C **54**, 1598 (1996).
[8] I. Thorslund, D. B. Fossan, D. R. LaFosse, H. Schnare, K. Hauschild, I. M. Hibbert, S. M. Mullins, E. S. Paul, I. Ragnarsson, J. M. Sears, P. Vaska, and R. Wadsworth, Phys. Rev. C **52**, R2839 (1995).
[9] I. Ragnarsson, V. P. Janzen, D. B. Fossan, N. C. Schmeing, and R. Wadsworth, Phys. Rev. Lett. **74**, 3935 (1995).
[10] A. V. Afanasjev and I. Ragnarsson, Nucl. Phys. **A591**, 387 (1995).
[11] R. Wadsworth, R. M. Clark, J. A. Cameron, D. B. Fossan, I. M. Hibbert, V. P. Janzen, R. Krucken, G. J. Lane, I. Y. Lee, A. O. Macchiavelli, C. M. Parry, J. M. Sears, J. F. Smith, A. V. Afanasjev, and I. Ragharsson, Phys. Rev. Lett. **80**, 1174 (1998).
[12] P. H. Regan, A. E. Stuchbery, G. D. Dracoulis, A. P. Byrne, G. J. Lane, T. Kibedi, D. C. Radford, A. Galindo-Uribarri, V. P. Janzen, D. Ward, S. M. Mullins, G. Hackman, J. H. DeGraaf, M. Cromaz, and S. Pilotte, Nucl. Phys. **A586**, 351 (1995).
[13] I. Thorslund, C. Fahlander, J. Nyberg, S. Juutinen, R. Julin, M. Piiparinen, R. Wyss, A. Lampinen, T. Lonnroth, D. Muller, S. Tormanen, and A. Virtanen, Nucl. Phys. **A564**, 285 (1993).
[14] S. Juutinen, R. Julin, M. A Piiparinen, P. Ahonen, B. Cederwall, C. Fahlander, A. Lampinen, T. Lonnroth, A. Maj, S. Mitarai, D. Muller, J. Nyberg, P. Simecek, M. Sugawara, I. Thorslund, S. Tormanen, A. Virtanen, and R. Wyss, Nucl. Phys. **A573**, 306 (1994).
[15] J. Kumpulainen, R. Julin, J. Kantele, A. Passoja, W. H. Trzaska, E. Verho, J. Vaaramaki, D. Cutoiu, and M. Ivascu, Phys. Rev. C **45**, 640 (1993).
[16] W. Satula and R. Wyss, Phys. Scr. **56**, 159 (1995).
[17] S. M. Mullins, V. P. Janzen, P. Vaska, D. B. Fossan, G. Hackman, D. R. LaFosse, E. S. Paul, D. Prévost, H. Schnare, J. C. Waddington, R. Wadsworth, D. Ward, and M. P. Waring, Phys. Lett. B **318**, 592 (1993).
[18] T. K. Alexander and J. S. Forster, in *Advances in Nuclear Physics*, edited by Michel Baranger and Erich Vogt (Plenum, New York, 1978), Vol. 10, Chap. 3.
[19] D. C. Radford, Nucl. Instrum. Methods Phys. Res. A **361**, 297 (1995).
[20] M. Conjeaud, S. Harar, and E. Thuriere, Nucl. Phys. **129**, 10 (1969).
[21] H. J. Kim and A. L. Robinson, Phys. Rev. C **9**, 767 (1974).
[22] W. Dietrich and A. Bäcklin, Z. Phys. A **276**, 133 (1976).
[23] W. H. A. Hesselink, J. Bron, P. M. A. van der Kam, V. Paar, A. van Poelgeest, and A. G. Zephat, Nucl. Phys. **A299**, 60 (1978).
[24] H. Takai, E. M. Takagui, and O. Dietzsch, Phys. Rev. C **37**, 571 (1988).
[25] D. Bucurescu, I. Cata-Danil, G. Ilas, M. Ivascu, N. Marginean, L. Stroe, and C. A. Ur, Phys. Rev. C **54**, 2313 (1996).
[26] K. S. Krane, R. M. Steffen, and R. M. Wheeler, Nucl. Data Tables **11**, 351 (1973).
[27] Evaluated Nuclear Structure Data File (ENSDF), maintained by the National Nuclear Data Center, Brookhaven National Laboratory.
[28] A. van Poelgeest, J. Bron, W. H. A. Hesselink, K. Allaart, J. J. A. Zalmstra, M. J. Uitzinger, and H. Verheul, Nucl. Phys. **A346**, 70 (1980).
[29] G. Bonsignori, M. Savoia, K. Allaart, A. van Egmond, and G. te Velde, Nucl. Phys. **A432**, 389 (1985).
[30] W. Nazarewicz, A. Johnson, and R. A. Wyss, Nucl. Phys. **A503**, 285 (1989).
[31] M. Piiparinen, R. Julin, S. Juutinen, A. Virtanen, P. Ahonen, C. Fahlander, J. Hattula, A. Lampinen, T. Lonnroth, A. Maj, S. Mitarai, D. Muller, J. Nyberg, A. Pakkanen, M. Sugawara, I. Thorslund, and S. Tormanen, Nucl. Phys. **A565**, 671 (1993).
[32] W. Dietrich, A. Backlin, C. O. Launnegard, and I. Ragnarsson, Nucl. Phys. **A253**, 429 (1975).
[33] A. V. Afanasjev and I. Ragnarsson (private communication).
[34] I. Thorslund, C. Fahlander, J. Nyberg, M. Piiparinen, R. Julin, S. Juutinen, A. Virtanen, D. Muller, H. Jensen, and M. Sugawara, Nucl. Phys. **A568**, 306 (1994).
[35] G. Baldsiefen, P. Maagh, H. Hubel, W. Korten, S. Chmel, M. Neffgen, W. Pohler, H. Grawe, K. H. Maier, K. Spohr, R. Schubart, S. Frauendorf, and H. J. Maier, Nucl. Phys. **A592**, 365 (1995).
[36] S. Frauendorf, in *Proceedings of the Workshop on Gammasphere Physics*, Berkeley, 1995 (World Scientific, Singapore, 1996), p. 272.
[37] S. Frauendorf. Nucl. Phys. **A557**, 259c (1993).
[38] S. Frauendorf and J. Reif, Nucl. Phys. **A621**, 736 (1997).